LETTER

doi:10.1038/nature13667

A microbial ecosystem beneath the West Antarctic ice sheet

Brent C. Christner[1], John C. Priscu[2], Amanda M. Achberger[1], Carlo Barbante[3], Sasha P. Carter[4], Knut Christianson[5]†, Alexander B. Michaud[2], Jill A. Mikucki[6], Andrew C. Mitchell[7], Mark L. Skidmore[8], Trista J. Vick-Majors[2] & the WISSARD Science Team‡

Liquid water has been known to occur beneath the Antarctic ice sheet for more than 40 years[1], but only recently have these subglacial aqueous environments been recognized as microbial ecosystems that may influence biogeochemical transformations on a global scale[2–4]. Here we present the first geomicrobiological description of water and surficial sediments obtained from direct sampling of a subglacial Antarctic lake. Subglacial Lake Whillans (SLW) lies beneath approximately 800 m of ice on the lower portion of the Whillans Ice Stream (WIS) in West Antarctica and is part of an extensive and evolving subglacial drainage network[5]. The water column of SLW contained metabolically active microorganisms and was derived primarily from glacial ice melt with solute sources from lithogenic weathering and a minor seawater component. Heterotrophic and autotrophic production data together with small subunit ribosomal RNA gene sequencing and biogeochemical data indicate that SLW is a chemosynthetically driven ecosystem inhabited by a diverse assemblage of bacteria and archaea. Our results confirm that aquatic environments beneath the Antarctic ice sheet support viable microbial ecosystems, corroborating previous reports suggesting that they contain globally relevant pools of carbon and microbes[2,4] that can mobilize elements from the lithosphere[6] and influence Southern Ocean geochemical and biological systems[7].

Almost 400 subglacial lakes have been identified beneath the Antarctic ice sheet[8]. Speculation on the presence of functional microbial ecosystems within these lakes followed their discovery[1] and motivated the initial studies of samples originating from Subglacial Lake Vostok (SLV)[9,10]. However, the body of microbiological data from SLV has been a point of contention, primarily because all studies were based on analyses of frozen (that is, accreted) lake water samples recovered from a borehole containing a contaminated hydrocarbon drilling fluid[3]. Our report documents the first analysis of water and surficial sediments collected directly from a subglacial lake beneath the West Antarctic ice sheet (WAIS) using microbiologically clean drilling and sampling techniques[11].

The water residence time for SLV exceeds 10,000 years[12], while that for 'active' lakes such as SLW is on the order of years to decades[5,8]. SLW is part of a network of three major reservoirs beneath the lower ice plain of the WIS that regulate water transport to a subglacial estuary at the grounding zone, linking the hydrological system to the sub-ice-ocean cavity beneath the Ross Ice Shelf[5,13] (Fig. 1). During two separate drainage events in 2006 and 2009, SLW discharged ~0.15 km^3 of water over two six-month periods, each time lowering the lake level by about 5 m[5,14]. The drilling location to access SLW was selected using reflection seismology[13] and ice-penetrating radar[14] data, and corresponded to the region of maximum predicted water column thickness, lowest hydropotential, and largest satellite-measured surface elevation changes (Fig. 1).

A hot water drilling system was used to create a ~0.6 m diameter borehole through the overlying ice sheet into SLW, allowing for physical measurements and the direct collection of water column and sediment samples. Drilling and lake entry procedures followed recommendations for environmental protection of subglacial aquatic environments[11], incorporating rigorous measures to reduce the introduction of foreign microbiota and material into SLW and the interconnected subglacial drainage

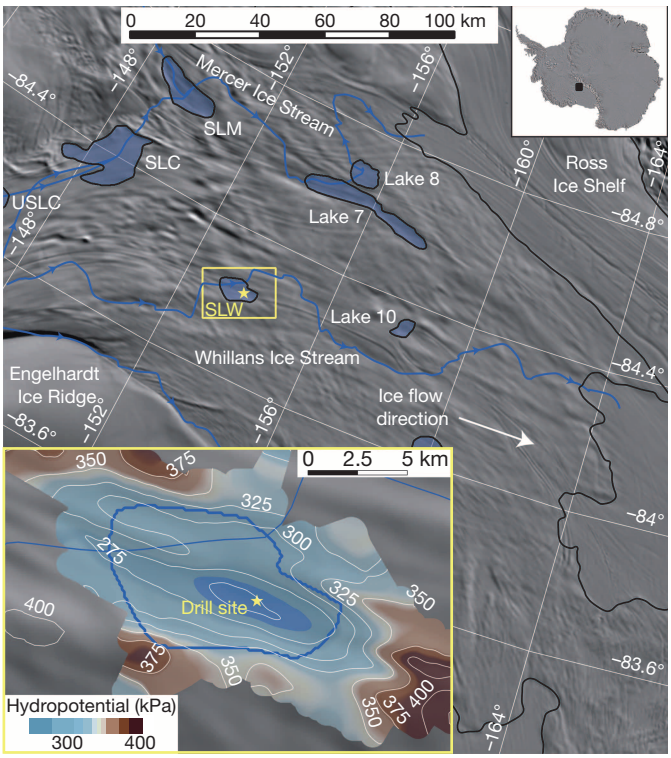

Figure 1 | Locator map of the WIS and SLW. The yellow box and star indicate the general location of the lake and the drill site; maximum extent of SLW and other lakes[28] under the ice stream are shaded in blue; predicted subglacial water flowpaths through SLW and other subglacial lakes are represented by blue lines with arrows; the black line denotes the ice-sheet grounding line at the edge of the Ross Ice Shelf[29]. Inset (expanded from area in yellow box) shows details of SLW with both maximum (solid blue line) and minimum lake extent (shaded blue area), hydropotential contours (white isolines; 25 kPa interval), and drill site (yellow star; 84.240° S 153.694° W). Background imagery is MODIS MOA[30].

[1]Department of Biological Sciences, Louisiana State University, Baton Rouge, Louisiana 70803, USA. [2]Department of Land Resources and Environmental Science, Montana State University, Bozeman, Montana 59717, USA. [3]Institute for the Dynamics of Environmental Processes – CNR, Venice, and Department of Environmental Sciences, Informatics and Statistics, Ca'Foscari University of Venice, Venice 30123, Italy. [4]Institute of Geophysics and Planetary Physics, Scripps Institution of Oceanography, University of California San Diego, La Jolla, California 92093, USA. [5]Physics Department, St Olaf College, Northfield, Minnesota 55057, USA. [6]Department of Microbiology, University of Tennessee, Knoxville, Tennessee 37996, USA. [7]Department of Geography and Earth Sciences, Aberystwyth University, Aberystwyth SY23 3DB, UK. [8]Department of Earth Science, Montana State University, Bozeman, Montana 59717, USA. †Present address: Courant Institute of Mathematical Sciences, New York University, New York, New York 10012, USA (K.C.).
‡Lists of participants and their affiliations appear at the end of the paper.

system. Video inspection of the borehole and temperature measurements revealed that the ice–water interface occurred at 801 ± 1 m below the surface (mbs) and the lake depth at the borehole site was ~2.2 m at the time of sampling. Two borehole deployments of a conductivity, temperature and depth (CTD) sonde together with data from three discrete hydrocasts showed that SLW had an average *in situ* temperature of −0.49 °C, pH of 8.1, and conductivity of 720 μS cm^{-1}; properties that were distinctly different from the borehole water (Table 1).

Water from three discrete hydrocasts in SLW had near identical geochemical compositions on the basis of major ion chemistry (Table 1) and all showed oxygen under-saturation (~16% of air-saturated water). Since there is no definitive evidence of lake water freezing to the bottom of the overlying ice sheet as in SLV[12], it is unlikely that lake water constituents in SLW are influenced significantly by freeze concentration. The $\delta^{18}O$ of H_2O for SLW (−38.0‰) was similar to glacial ice sampled approximately 10 m above the ice–water interface from the neighbouring Kamb Ice Stream[15] (KIS; −38 to −39‰), indicating that glacial melt was the dominant water source for SLW. A considerable fraction of the major anions and cations originated from mineral weathering, with a minor seawater component based on Cl^- to Br^- ratios (Extended Data Table 1). Crustally derived non-seawater solutes in SLW showed a dominance of weathering products from silicate minerals ($Na^+ + K^+$) over carbonate minerals ($Mg^{2+} + Ca^{2+}$), similar to other sub ice-sheet systems in Greenland and Antarctica[6,7] (Supplementary Discussion). The dominant non-seawater anions (SO_4^{2-} and HCO_3^-) were probably products of sulphide oxidation, carbonation reactions, and carbonate dissolution[7]. Sulphide oxidation and carbonation reactions have been demonstrated to be microbially driven in subglacial systems and linked to enhanced rates of mineral weathering[16]. Although clay minerals are a potential source of the relatively high F^- concentrations in SLW (Table 1), subglacial volcanism in the upstream catchment supplying SLW[17] may also contribute.

Table 1 | Biogeochemical data from the SLW borehole, water column, and surficial sediments

Parameter	Borehole*	Water column†	Sediments‡
Physical			
Temperature (°C)§	−0.17 (0.25)	−0.49 (0.03)	n.d.
Conductivity (μS cm^{-1} @ 25 °C)‖	5.3	720 (10)	860
pH‖	5.4	8.1 (0.1)	7.3
Redox (mV (SHE))‖	n.d.	382	n.d.
Microbiological			
Cell density (cells ml^{-1})	6.9×10^2 (51.0)	1.3×10^5 (0.4×10^5)	n.d.
Cellular ATP (pmol l^{-1})	0.04 (0.002)	3.70 (1.00)	n.d.
[^{3}H]thymidine¶	n.d.	13.7 (1.3)	46.6 (5.6)
[^{3}H]leucine¶	n.d.	2.9 (0.4)	0.9 (0.04)
^{14}C-bicarbonate (ng C l^{-1} d^{-1})	n.d.	32.9 (4.2)	n.d.
Carbon and nutrients			
Dissolved oxygen (μmol l^{-1})	n.d.	71.9 (12.5)	n.d.
DIC (mmol l^{-1})	n.d.	2.11 (0.03)	n.d.
DOC (μmol l^{-1})	n.d.	221 (55)	n.d.
Acetate (μmol l^{-1})	n.d	1.3 (0.2)	n.d.
Formate (μmol l^{-1})	n.d	1.2 (0.3)	n.d.
PC#	n.d.	78.5 (7.4)	384.2 (37.0)
PN#	n.d.	1.2 (0.4)	21.5 (1.7)
PC:PN (molar)	n.d.	65.4 (0.3)	17.9 (0.4)
NH_4^+ (μmol l^{-1})	n.d.	2.4 (0.6)	n.d.
NO_2^- (μmol l^{-1})	n.d.	0.1 (0.1)	n.d.
NO_3^- (μmol l^{-1})	n.d.	0.8 (0.5)	9.1
PO_4^{3-} (μmol l^{-1})	n.d.	3.1 (0.7)	7.3
DIN:SRP (molar)	n.d.	1.1 (0.4)	n.d.
Major ions (μeq l^{-1})			
Na^+	n.d.	5,276 (18)	6,977
K^+	n.d.	186 (4.2)	293 (1.0)★
Mg^{2+}	n.d.	507 (12)	596 (101)★
Ca^{2+}	n.d	859 (29)	860 (104)★
F^-	n.d.	31.5 (0.4)	34.0
Cl^-	n.d.	3,537 (3.4)	4,943
Br^-	n.d.	6 (0.01)	7 (0.4)★
SO_4^{2-}	n.d.	1,111 (0.4)	1,230
HCO_3^-	n.d	2,111 (35)	2,238**
Stable isotopes††			
$\delta^{18}O$ of H_2O	n.d.	−38.0‰	−37.5‰
$\Delta^{17}O$ of NO_3^-	n.d.	−0.1 to 0.2‰	n.d.

* Borehole water sampled by hydrocast at 672 mbs before lake entry.
† Water column data represent averages (± s.d.) from hydrocasts collected on 28 January 2013 (cast 1), 30 January (cast 2) and 31 January (cast 3) 2013, except for [^{3}H]leucine incorporation, which is an average of cast 1 and 3 only.
‡ The sediment data correspond to measurements from the upper 2 cm of surficial sediments.
§ Average (± s.d.) of *in situ* measurements made through the lake water column at ~10 cm intervals with a SBE 19*plus*V2 SeaCAT Profiler CTD on 28 January and 30 January 2013.
‖ Based on measurements from discrete water samples brought to the surface.
¶ Macromolecular incorporation rates of tritium were converted to cellular carbon and presented along with bicarbonate incorporation as average ng C l^{-1} d^{-1} (± s.d.) for water or average ng C d^{-1} gram dry weight $^{-1}$ (± s.d.) of sediment.
# Average (± s.d.) μmol l^{-1} for water and average (± s.d.) μmol g dry weight sed^{-1} for surficial sediment.
★ Surficial sediment porewater major ions are the average (± range) of two replicates.
** Calculated based on charge balance.
†† Values are per thousand and reported relative to V-SMOW. The range of 2 measurements is given for $\Delta^{17}O$ of NO_3^-.
n.d., no data available.

Ammonium accounted for 73% of the dissolved inorganic nitrogen pool within the water column of SLW (Table 1). Given that mineral sources of ammonium are minor, the majority of the ammonium is probably from microbial mineralization. Soluble reactive phosphorus levels were similar to the total inorganic nitrogen pool (dissolved N:P molar ratio of 1.1), implying a biologically nitrogen-deficient environment, relative to phosphorus. Unfortunately, sample limitations precluded measurement of dissolved organic N and P concentrations to assess their nutritional contribution. In addition to its nutritional role, ammonium is also an energy source for chemolithoautotrophic ammonium-oxidizing bacteria and archaea. Evidence for complete nitrification in the aerobic SLW water column was supported by $\Delta^{17}O$ of NO_3 values (−0.1‰ to 0.2‰) that indicated microbial processes rather than atmospheric input was the dominant source for nitrate in the lake[18]. Particulate organic C (PC) to N (PN) molar ratios in the water column exceeded that of actively growing bacteria by almost 15-fold, suggestive of elevated levels of nitrogen-poor detritus. Dissolved organic carbon (DOC) in the water column averaged 221 ± 55 μmol l^{-1}, which is about five times greater than average values for the deep ocean[19] and similar to the maximum range estimate for SLV[9,20] (86–160 μmol l^{-1}). Acetate and formate concentrations in the water column averaged 1.3 and 1.2 μmol l^{-1}, respectively, indicating that at least a portion of the DOC pool was labile. The conductivity and microbiological data (Table 1 and Fig. 2a) showed that little mixing occurred between the borehole water and lake, supporting the hypothesis that DOC in the water column originated from SLW. The lack of winnowing in sediment cores from SLW, in concert with the fact that similar DOC concentrations were obtained as the overlying ice moved ~4 m during the course of our operations, provided evidence that water column DOC did not result from sediment disturbance during drilling operations. The DOC in SLW most likely originated from upward diffusion of DOC associated with ancient marine sediments[4] (SLW sediment surface area:depth ratio ≈ 30,000), chemoautotrophic production, or from a combination of both sources.

The average cell density in the SLW water column was 1.3×10^5 cells ml^{-1} (Table 1); microscopy revealed the presence of numerous morphotypes, approximately 10% of which were filamentous (Fig. 3). Cellular ATP, a proxy for viable biomass, in SLW was 3.7 pmol ATP l^{-1} (Table 1). Cell and ATP concentrations were 188- and 93-fold higher, respectively, than those observed in the borehole water before breakthrough to SLW. Carbon biomass estimates for SLW water based on the ATP data (480 ± 100 ng C l^{-1}) were 3- to 50-fold higher than those observed beneath the Ross Ice Shelf at site J9 (ref. 21). Analysis of small subunit ribosomal RNA (SSU rRNA) sequences amplified from the water column samples showed that the community was similar among replicate lake samples, was distinct from the drilling water (Fig. 2a), and contained at least 3,931 operational taxonomic units (OTUs; Extended Data Table 2). An OTU closely related to the nitrite oxidizing betaproteobacterium '*Candidatus* Nitrotoga arctica'[22] comprised 13% of the sequence data, and many of the most abundant phylotypes were closely related to chemolithoautotrophic species that use reduced nitrogen, iron or sulphur compounds as energy sources (Fig. 2b; Supplementary Discussion). Two of

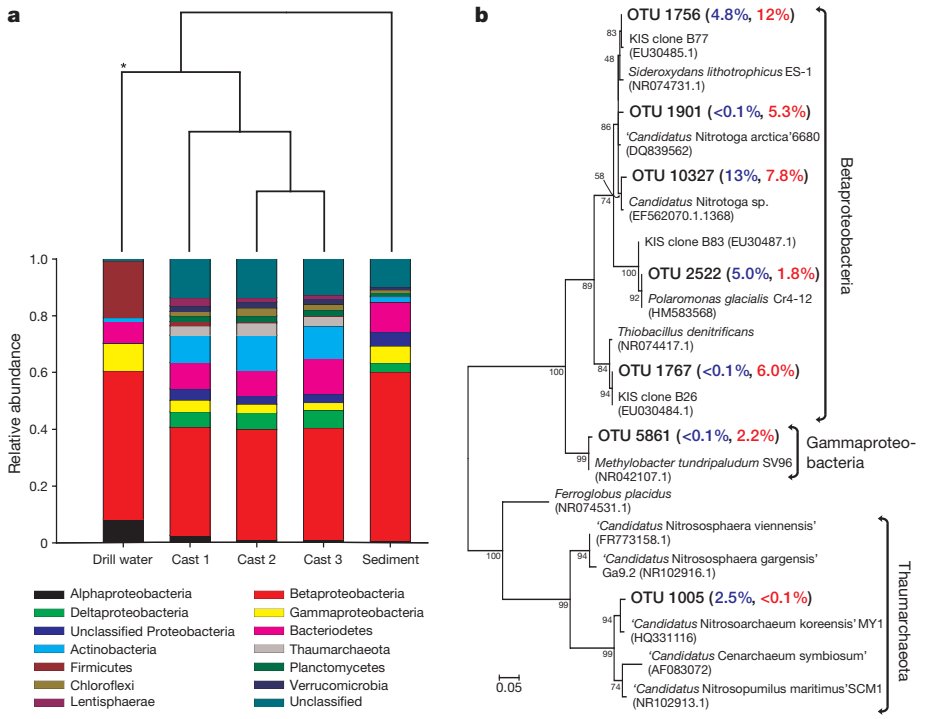

Figure 2 | Phylogenetic analysis of SSU gene sequences obtained from the SLW water column, surficial sediment (0–2 cm) and drilling water. **a**, Cluster analysis of the microbial phylogenetic structure in the samples (top) and the relative abundance of bacterial and archaeal phyla in the water and sediment samples (bottom). The Proteobacteria were split into classes for greater detail. The asterisk indicates statistical significance (analysis of molecular variance, AMOVA, P value < 0.001). **b**, Phylogenetic analysis of bacterial and archaeal OTUs abundant in the SLW water column and sediments. The accession numbers of nearest neighbours and reference taxa are listed parenthetically. Bootstrap values are shown at the nodes. SLW phylotypes are bolded and followed by the percentage each represented in the water column (blue) and sediment (red) libraries. The scale bar indicates the number of nucleotide substitutions per position.

the abundant water column OTUs had high identity (>99%) to SSU sequences previously reported from sediments sampled beneath the KIS[23] (Fig. 2b). Preliminary attempts to detect eukaryotic SSU sequences in the SLW water column were unsuccessful.

Average dark [^{14}C]bicarbonate incorporation in the water column samples (32.9 ng C l^{-1} d^{-1}; Table 1) exceeded average rates of heterotrophic production based on [^{3}H]thymidine (13.7 ng C l^{-1} d^{-1}) and [^{3}H]leucine (2.9 ng C l^{-1} d^{-1}) incorporation by 2- and 11-fold, respectively. Assuming that the thymidine and leucine values represent net incorporation, and that respiratory losses were 87% of net incorporation (which are average values for Antarctic McMurdo Dry Valley lakes[24]), the gross bacterial carbon demand (net productivity + respiration) would be 105 and 23 ng C l^{-1} d^{-1}, respectively. If dark [^{14}C]bicarbonate incorporation represents new organic carbon production via chemoautotrophy, the observed rates would meet between 31% and 143% of the heterotrophic carbon demand in the system. It should be noted that the effect of pressure (~ 8 MPa in SLW) was not tested and may influence the absolute rates of metabolism measured.

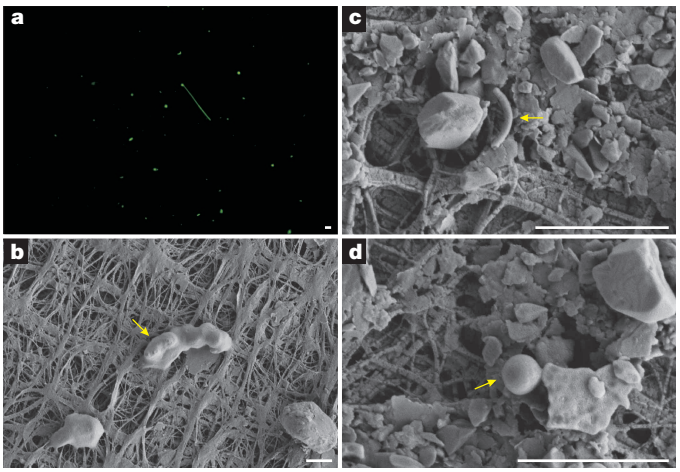

Figure 3 | Morphological diversity of microbial cells in the SLW water column. **a**, Epifluorescence micrograph showing a variety of cell morphotypes, which was confirmed by scanning electron microscopy (SEM; **b**–**d**). The yellow arrows in the SEM images indicate cells with rod (**b**), curved rod (**c**) and coccoid (**d**) morphologies. Scale bar, 2 μm.

Pore water conductivity (860 μS cm^{-1}) and pH (7.3) in SLW's surficial sediments were within 20% of the lake water values (Table 1). Upward diffusion of ions from sediment pore water is presumably the primary source of the ions in the water column. Average surficial sediment PC and PN concentrations were 384.2 and 21.5 μmol g dry weight^{-1}, respectively, and represented 0.43% and 0.03% of sediment dry weight. The molar PC:PN ratio in the surficial sediment layer (17.9) was 3.7-fold lower than that in the water column (Table 1), indicative of nitrogen-enriched sedimentary particulate organic matter, with respect to water column suspensoids. On the basis of rates of thymidine and leucine incorporation, average heterotrophic production in the surficial sediment was 46.6 and 0.9 ng C d^{-1} g dry weight^{-1}, respectively. Approximately 75% of the OTUs from the surficial sediments classified within the Proteobacteria (Fig. 2a). Although many phylotypes in the water column were also abundant in the surficial sediments (Fig. 2b), ~70% of the OTUs were unique to the sediment environment. The nearest neighbours of the most abundant phylotypes in the surface sediments were chemolithoautotrophs or species that use C1 hydrocarbons as carbon and energy sources (Fig. 2b, Supplementary Discussion).

Our data show that SLW supports a metabolically active and phylogenetically diverse ecosystem that functions in the dark at sub-zero temperatures, confirming more than a decade of circumstantial evidence regarding the presence of life beneath Antarctica's ice sheet[9,10,20,23]. Rate experiments revealed that chemoautotrophic primary production in SLW

is adequate to support heterotrophic metabolism in the subglacial ecosystem. The abundance of taxa related to nitrifiers[22,25] in concert with elevated ammonium and $\Delta^{17}O$ of NO_3 values near 0‰ in the water column (Table 1) implies that nitrification may be a fundamental chemoautotrophic pathway of new organic carbon production in SLW. Similar conclusions regarding the ecological significance of nitrification have been drawn for the water column beneath the Ross Ice Shelf[26] and in McMurdo Sound[27]. Given the prevalence of subglacial water in Antarctica[8], our data from SLW lead us to contend that aquatic microbial ecosystems are common features of the subsurface environment that exists beneath the $\sim 10^7$ km^2 Antarctic ice sheet.

Online Content Methods, along with any additional Extended Data display items and Source Data, are available in the online version of the paper; references unique to these sections appear only in the online paper

Received 2 April; accepted 9 July 2014.

1. Oswald, G. K. A. & De Robin, G. Q. Lakes beneath the Antarctic ice sheet. *Nature* **245,** 251–254 (1973).
2. Priscu, J. C. *et al.* in *Polar Lakes and Rivers* (eds Vincent, W. & Laybourn-Parry, J.) Ch.7 (Oxford Univ. Press, 2008).
3. Christner, B. C., Skidmore, M. L., Priscu, J. C., Tranter, M. & Foreman, C. M. in (eds Margesin, R., Schinner, F., Marx., J.-C. & Gerday, C.) *Psychrophiles: From Biodiversity to Biotechology* pp. 51–71 (Springer, 2008).
4. Wadham, J. L. *et al.* Potential methane reservoirs beneath Antarctica. *Nature* **488,** 633–637 (2012).
5. Fricker, H. A., Scambos, T., Bindschadler, R. & Padman, L. An active subglacial water system in West Antarctica mapped from space. *Science* **315,** 1544–1548 (2007).
6. Skidmore, M., Tranter, M., Tulaczyk, S. & Lanoil, B. Hydrochemistry of ice stream beds–evaporitic or microbial effects? *Hydrol. Processes* **24,** 517–523 (2010).
7. Wadham, J. L. *et al.* Biogeochemical weathering under ice: size matters. *Glob. Biogeochem. Cycles* **24,** GB3025 (2010).
8. Wright, A. & Siegert, M. A fourth inventory of Antarctic subglacial lakes. *Antarct. Sci.* **24,** 659–664 (2012).
9. Priscu, J. C. *et al.* Geomicrobiology of subglacial ice above Lake Vostok. *Science* **286,** 2141–2144 (1999).
10. Karl, D. M. *et al.* Microorganisms in the accreted ice of Lake Vostok. *Science* **286,** 2144–2147 (1999).
11. Priscu, J. C. *et al.* A microbiologically clean strategy for access to the Whillans Ice Stream subglacial environment. *Antarct. Sci.* **25,** 637–647 (2013).
12. Bell, R. E. *et al.* Origin and fate of Lake Vostok water frozen to the base of the East Antarctic ice sheet. *Nature* **416,** 307–310 (2002).
13. Horgan, H. J. *et al.* Estuaries beneath ice sheets. *Geology* **41,** 1159–1162 (2013).
14. Christianson, K., Jacobel, R. W., Horgan, H. J., Anandakrishnan, S. & Alley, R. B. Subglacial Lake Whillans—Ice-penetrating radar and GPS observations of a shallow active reservoir beneath a West Antarctic ice stream. *Earth Planet. Sci. Lett.* **331–332,** 237–245 (2012).
15. Vogel, S. W. *et al.* Subglacial conditions during and after stoppage of an Antarctic ice stream: is reactivation imminent? *Geophys. Res. Lett.* **32,** L14502 (2005).
16. Montross, S. N., Skidmore, M., Tranter, M., Kivimäki, A.-L. & Parkes, R. J. A microbial driver of chemical weathering in glaciated systems. *Geology* **41,** 215–218 (2013).
17. Blankenship, D. D. *et al.* Active volcanism beneath the West Antarctic ice-sheet and implications for ice-sheet stability. *Nature* **361,** 526–529 (1993).
18. Michalski, G., Bhattacharya, S. K. & Girsch, G. NO_x cycle and tropospheric ozone isotope anomaly: an experimental investigation. *Atmos. Chem. Phys. Discuss.* **13,** 9443–9483 (2013).
19. Hansell, D. A. & Carlson, C. A. Deep-ocean gradients in the concentration of dissolved organic carbon. *Nature* **395,** 263–266 (1998).
20. Christner, B. C. *et al.* Limnological conditions in Subglacial Lake Vostok, Antarctica. *Limnol. Oceanogr.* **51,** 2485–2501 (2006).
21. Azam, F. *et al.* Occurrence and metabolic activity of organisms under the Ross Ice Shelf, Antarctica, at Station J9. *Science* **203,** 451–453 (1979).
22. Alawi, M., Lipski, A., Sander, T., Pfeiffer, E.-M. & Spieck, E. Cultivation of a novel cold-adapted nitrite oxidizing betaproteobacterium from the Siberian Arctic. *ISME J.* **1,** 256–264 (2007).
23. Lanoil, B. *et al.* Bacteria beneath the West Antarctic ice sheet. *Environ. Microbiol.* **11,** 609–615 (2009).
24. Takacs, C., Priscu, J. & McKnight, D. Bacterial dissolved organic carbon demand in McMurdo Dry Valley Lakes, Antarctica. *Limnol. Oceanogr.* **46,** 1189–1194 (2001).
25. Walker, C. B. *et al. Nitrosopumilus maritimus* genome reveals unique mechanisms for nitrification and autotrophy in globally distributed marine crenarchaea. *Proc. Natl Acad. Sci. USA* **107,** 8818–8823 (2010).
26. Horrigan, S. G. Primary production under the Ross Ice Shelf, Antarctica. *Limnol. Oceanogr.* **26,** 378–382 (1981).
27. Priscu, J. C., Downes, M. T., Priscu, L. R., Palmisano, A. C. & Sullivan, C. W. Dynamics of ammonium oxidizer activity and nitrous oxide (N_2O) within and beneath Antarctic sea ice. *Mar. Ecol. Prog. Ser.* **62,** 37–46 (1990).
28. Fricker, H. A. & Scambos, T. Connected subglacial lake drainage activity on lower Mercer and Whillans Ice Streams, West Antarctica, 2003–2008. *J. Glaciol.* **55,** 303–315 (2009).
29. Depoorter, M. A. *et al.* Calving fluxes and basal melt rates of Antarctic ice shelves. *Nature* **502,** 89–92 (2013).
30. Haran, T., Bohlander, J., Scambos, T. & Fahnestock, M. MODIS mosaic of Antarctica (MOA) image map. http://dx.doi.org/10.7265/N5ZK5DM5 (National Snow and Ice Data Center, 2005).

Supplementary Information is available in the online version of the paper.

Acknowledgements The Whillans Ice Stream Subglacial Access Research Drilling (WISSARD) project was funded by National Science Foundation grants (0838933, 0838896, 0838941, 0839142, 0839059, 0838885, 0838855, 0838763, 0839107, 0838947, 0838854, 0838764 and 1142123) from the Division of Polar Programs. Partial support was also provided by funds from NSF award 1023233 (B.C.C.), NSF award 1115245 (J.C.P.), the NSF's Graduate Research Fellowship Program (1247192; A.M.A.), the Italian National Antarctic Program (C.B.), and fellowships from the NSF's IGERT Program (0654336) and the Montana Space Grant Consortium (A.B.M.). Logistics were provided by the 139th Expeditionary Airlift Squadron of the New York Air National Guard, Kenn Borek Air, and by many dedicated individuals working as part of the Antarctic Support Contractor, managed by Lockheed-Martin. The drilling was directed by F. Rack; D. Blythe, J. Burnett, C. Carpenter, D. Duling (chief driller), D. Gibson, J. Lemery, A. Melby and G. Roberts provided drill support at SLW. L. Geng, B. Vandenheuvel, A. Schauer and E. Steig provided assistance with the stable isotopic analyses. We thank J. Dore for assistance with the nutrient analysis.

Author Contributions The manuscript was written by B.C.C. and J.C.P.; A.M.A. generated and analysed the molecular data; C.B., A.C.M. and M.L.S. conducted and interpreted the chemical measurements; S.P.C. and K.C. provided geophysical data; J.A.M. obtained and examined the CTD data; A.B.M. and T.J.V. contributed and analysed physiological and biogeochemical data; M.L.S. conducted and interpreted the isotopic analyses; and T.J.V. provided the micrographs. All authors contributed to the study design and acquisition of samples and/or data.

Author Information The SSU sequence data are deposited in the NCBI SRA database under the accession number SRP041285. Reprints and permissions information is available at www.nature.com/reprints. The authors declare no competing financial interests. Readers are welcome to comment on the online version of the paper. Correspondence and requests for materials should be addressed to B.C.C. (xner@lsu.edu) or J.C.P. (jpriscu@montana.edu).

WISSARD Science Team Members

W. P. Adkins[1], S. Anandakrishnan[2], G. Barcheck[3], L. Beem[3], A. Behar[4], M. Beitch[3], R. Bolsey[3], C. Branecky[3], R. Edwards[5], A. Fisher[3], H. A. Fricker[6], N. Foley[3], B. Guthrie[7], T. Hodson[7], R. Jacobel[8], S. Kelley[5], K. D. Mankoff[3], E. McBryan[4], R. Powell[7], A. Purcell[9], D. Sampson[3], R. Scherer[7], J. Sherve[5], M. Siegfried[6] & S. Tulaczyk[3]

[1]Department of Biological Sciences, Louisiana State University, Baton Rouge, Louisiana 70803, USA. [2]Department of Geosciences, Pennsylvania State University, University Park, Pennsylvania 16802, USA. [3]Department of Earth and Planetary Sciences, University of California, Santa Cruz, Santa Cruz, California 95064, USA. [4]School of Earth and Space Exploration, Arizona State University, Tempe, Arizona 85287, USA. [5]Department of Land Resources and Environmental Science, Montana State University, Bozeman, Montana 59717, USA. [6]Institute of Geophysics and Planetary Physics, Scripps Institution of Oceanography, University of California San Diego, La Jolla, California 92093, USA. [7]Department of Geology and Environmental Geosciences, Northern Illinois University, DeKalb, Illinois 60115, USA. [8]Physics Department, St Olaf College, Northfield, Minnesota 55057, USA. [9]Department of Microbiology, University of Tennessee, Knoxville, Tennessee 37996, USA.

METHODS

Site selection and description. SLW was discovered using satellite laser altimetry and initially identified as a region ($59 \pm 12\,km^2$) of temporally varying surface elevation; it is one of 11 active subglacial lakes documented beneath the WIS[5]. SLW fills and drains every few years as part of a series of hydrologically linked subglacial lakes in the area, eventually draining to the ocean[5,28,31]. Ice-penetrating radar and active-source seismic data estimated that the maximum lake depth does not exceed 8 and 15 m at low- and high-stand, respectively[14,32]. A lake-level rise of ~5 m from the low-stand lake level plus ice-flexural effects are sufficient to initiate flow over a drainage divide and trigger lake drainage. During a drainage event, ~0.15 km^3 of water drains in a six-month timeframe at a water flux of ~10 $m^3\,s^{-1}$ (refs 5, 14). Thus, SLW is a shallow active hydrological reservoir beneath an active ice stream. The deepest point in the seismically detected water column was selected as the drill site (84.240° S 153.694° W; Fig. 1). Drilling and subglacial lake access occurred during a near low-stand state in late January 2013[33].

Hot water drilling and clean access to SLW. A hot water drilling system was used between 23–27 January 2013 to melt through the ~801 m thick ice sheet, creating an access borehole (minimum diameter ~60 cm) for direct sampling and to conduct *in situ* measurements of the SLW water column and sediments. Microbial cells in the drilling water and on exposed surfaces of the hose, cables, and deployed equipment were reduced and killed through the use of four complementary technologies: (1) filtration, (2) ultraviolet irradiation, (3) pasteurization, and (4) disinfection with 3% w/v H_2O_2 (ref. 11). The drilling water, derived from the overlying ice sheet, was continuously circulated through a water treatment system that removed micron and sub-micron sized particles (>0.2 μm), irradiated the drilling water with two germicidal wavelengths of ultraviolet radiation (185 nm ~40,000 $\mu W\,s^{-1}\,cm^{-2}$ and 254 nm ~175,000 $\mu W\,s^{-1}\,cm^{-2}$), and pasteurized the water at 90 °C to reduce the viability of persisting microbial contamination. Ports were plumbed along the system's flow path, allowing discrete water samples to be obtained before and after each stage[11]. The drill hose and instrument cables were deployed at a rate no greater than 1 $m\,s^{-1}$ through a custom borehole collar that contained 12 amalgam pellet ultraviolet lamps, providing a cumulative germicidal ultraviolet dosage of at least 40,000 $\mu W\,s^{-1}\,cm^{-2}$ (Arapahoe SciTech). All borehole sampling tools and instruments were spray-saturated with 3% w/v H_2O_2 and staged in sealed polyethylene bags until tool deployment. Single-use protective apparel (Tyvek) was worn by all personnel during borehole science operations. The efficacy of the clean access technology and procedures were tested thoroughly before use in the field and are detailed elsewhere[11].

Drilling was conducted at a flow rate of ~135 l min^{-1} to ~700 mbs, whereupon the drill was withdrawn, the borehole was inspected with video, and a hydrocast was conducted at 672 mbs to measure the chemical and microbiological properties of the borehole water. To ensure that borehole water did not enter the lake upon breakthrough, the borehole hydrostatic pressure was reduced by ~35% (that is, the water level was lowered from 80 to 108 mbs) below the expected equilibration level for 800 m of ice[14]. Drilling subsequently proceeded at the reduced flow rate of 19 l min^{-1}, and at 08:02 on 27 January (UTC+12), the load on the hose diminished as the drill reached ~801 mbs. Two minutes later, the head above the borehole water return pump (stationed at 110 mbs) rose rapidly and remained at ~80 mbs, confirming hydrostatic equilibration between the borehole and lake water (that is, breakthrough to SLW). Importantly, the rise in borehole water confirmed that no drilling water entered the subglacial environment during breakthrough. To maintain the borehole and offset freeze back, thermal energy was added to the borehole by redeploying the drill at a flow rate of ~135 l min^{-1}. Borehole reaming was conducted after breakthrough to the lake by slowly withdrawing the drill (~1 m min^{-1}). A second 24 h reaming occurred 32 h after initial penetration of the lake to ensure successful deployment of all sampling tools. All *in situ* measurements and discrete sampling occurred over a 3-day period.

Temperature and depth. A SBE 19*plus*V2 SeaCAT Profiler CTD (Seabird Electronics, Inc.) was used to measure temperature and depth within the borehole and lake water column. The instrument was deployed in profiling mode and lowered at a rate of ~0.5 $m\,s^{-1}$. Borehole depths are referenced to the snow surface in proximity to the borehole. The water column depth in SLW (that is, the distance between the ice–water interface and underlying sediments) was estimated using CTD data to distinguish differences in water mass upon entry to the lake water column from the borehole. Lake depth was obtained from the top of the lake water mass to the depth where the sonde contacted the bottom. This depth estimate was corroborated with a calibrated cable attached to a real-time borehole video camera.

Water and sediment sampling. Following ref. 11, discrete samples of the drilling water (~20 l) were obtained at two time points during the drilling process. Samples of water from the input to the filtration module, input to the borehole, water returning from the borehole, and a hydrocast at 672 mbs before lake entry were collected and concentrated onto 142 mm 0.2 μm Supor membrane filters (Pall Corporation). The filters were processed identically to those from the SLW water column (see below).

Three discrete water samples were collected between 28 and 31 January 2013 at approximately mid-depth in the ~2.2 m SLW water column. Bulk water was collected using 10 l Niskin bottles and transferred via acid (10% HCl) leached silicon tubing to clean bottles following the limnological procedures outlined by the McMurdo Long Term Ecological Research (LTER) Program[34].

SLW water column particulate matter for nucleic acid analysis was filter concentrated *in situ* using a Large Volume Water Transfer System (WTS-LV) that was modified to fit the minimum borehole diameter of 30 cm (McLane Research Laboratories Inc.). The WTS-LV has a 3-tier 142 mm filter holder that accepts filters in series for size fractionation of particulates in the sample water. There were three separate casts of the WTS-LV in SLW and between 4.9 and 7.2 l of water was filter-concentrated during each 2 h deployment. In cast 1, the filter housing was loaded with a 10 μm nylon mesh screen together with 3 μm and 0.2 μm Supor membrane filters. The filters for cast 2 and 3 had pore sizes of 3.0 μm, 0.8 μm, and 0.2 μm. Immediately after recovery, the filter housing unit was detached from the pump and opened in a class 100 laminar flow hood. The filters were placed in sterile 142 mm Petri dishes, sliced into quarters with a clean scalpel, and transferred to a cryovial that contained 7 ml of DNA lysis solution (40 mM EDTA pH 8.0, 50 mM Tris pH 8.3, 0.73 M sucrose). The preserved samples were immediately frozen for transport to McMurdo Station and stored at −80 °C.

Surficial sediments were collected using a multicoring device (Uwitec) that had a core barrel inner diameter of 59.5 mm. Sediment pore water was obtained by inserting Rhizon samplers[35] (0.2 μm pore size) through predrilled holes in the core barrel liner and extracted under negative pressure created with a 10 ml sterile syringe. Surficial sediment (0 to 2 cm depth) from the cores was sampled inside a class 100 clean hood using a cleaned core cutter (Uwitec). The sediment samples for molecular biological analysis were placed in 60 ml sterile Nalgene bottles containing 10 ml of the DNA lysis solution and frozen.

Specific electrical conductivity (at 25 °C) and pH of the lake and sediment pore water were determined using a YSI model 3252 probe connected to a YSI model 3100 conductivity meter and a Beckman model 200 pH meter. Both probe and meter combinations were calibrated immediately before sample measurements were made.

Inorganic and organic chemistry. Particulate organic C (PC) and N (PN) samples from the water column were vacuum (~0.3 atm) filtered onto pre-combusted (450 °C for 4 h) Whatman GF/F filters and analysed on a CE Instruments Flash EA 112 (ThermoQuest, San Jose, CA). The filters and sediment samples which had been dewatered via centrifugation were fumed for 24 h over fresh 12 M HCl to remove inorganic carbon and dried for 24 h at 90 °C before analysis. Dissolved oxygen was measured using the azide modification of the mini-Winkler titration[36]. Dissolved inorganic carbon was measured by infrared gas analysis of acid sparged samples. Samples for dissolved inorganic N and P were filtered through pre-combusted and 1% v/v HCl leached GF/F filters, collected in 1% HCl leached HDPE bottles, and frozen for shipment to the US where nitrate, nitrite, ammonium, and soluble reactive P were analysed colorimetrically[34]. Major ions and organic acids from SLW water and sediment porewater were analysed on a Metrohm ion chromatograph using a C4 cation column and an aSupp5 anion column.

Stable isotope analysis. Stable isotope measurements were conducted at the Isolab (University of Washington, Seattle). Measurements of oxygen isotope ratios of lake water and pore water samples were made using a Picarro cavity ring-down laser spectrometer. Nitrate for $\Delta^{17}O$ determination in the water samples was concentrated using an anionic resin[37] followed by the bacterial reduction and thermal decomposition method[38,39]. $\Delta^{17}O$ of NO_3 was analysed with a Finnigan Delta Plus Advantage isotope ratio mass spectrometer. Isotope measurements are reported using standard δ notation in per thousand relative to Vienna Standard Mean Ocean Water (VSMOW).

pH and oxidation-reduction measurements. Sediment pH was measured with a Microelectrodes Inc. MI-407P needle pH electrode and a MI 401 $Ag/AgCl_2$ micro reference electrode, calibrated with Orion low ionic strength buffers (pH 4, 7, 10). Oxidation-reduction potential (ORP) was measured in SLW water with a glass epoxy platinum electrode and a MI 401 $Ag/AgCl_2$ micro reference electrode calibrated with Zobell's solution and corrected to the standard hydrogen electrode (SHE).

Cell and ATP concentration. Samples for cell enumeration from water and sediment were collected in combusted glass bottles and fixed in sodium borate-buffered formalin (2% v/v). Sub-samples were filtered on black 0.2 μm polycarbonate membrane filters, stained with SYBR Gold (Life Technologies), and immediately counted via epifluorescence microscopy. Sediment interference did now allow accurate determination of cell density in sediment samples. Cellular ATP was measured in triplicate as previously described[11] and viable biomass was estimated from the ATP concentration using a carbon to ATP ratio of 250 by weight[10,21].

Scanning electron microscopy. Samples for scanning electron microscopy (SEM) were fixed with either 2% (w/v) formalin or 0.5% (w/v) glutaraldehyde and filtered

onto a 13 mm diameter 0.2 μm polytetrafluoroethylene (PTFE) filters. Following ethanol dehydration and critical point drying, the filters were attached to an aluminium stub, coated with either gold or palladium, and observed on a Zeiss Supra 55VP Field Emission Scanning Electron Microscope.

Heterotrophic and chemoautotrophic production. Heterotrophic productivity was measured using [^{3}H]methyl-thymidine incorporation into DNA[40] and [^{3}H] leucine incorporation into protein[41]. Samples (1.5 ml; 10 and 5 live and 10 and 5 trichloroacetic acid (TCA)-killed controls for casts 1 and 3, respectively) were incubated with 20 nM radiolabelled thymidine (specific activity 20 Ci mmol^{-1}) or leucine (specific activity 84 Ci mmol^{-1}) at 4 °C in the dark for 175 h (average). A separate time-course experiment (data not shown) revealed that incorporation was linear over this incubation period. Incubations were terminated by the addition of 100% w/v cold TCA (5% final). Following centrifugation, a series of washes with cold 5% w/v TCA and cold 80% v/v ethanol were performed. The final pellet was dried overnight at ~25 °C. Radioactivity in the pellet was determined with a calibrated liquid scintillation counter following the addition of 1 ml of Cytoscint ES (MP Biomedicals). The rates of thymidine and leucine incorporation (nM TdR d^{-1} or nM Leu d^{-1}) obtained at the incubation temperature (4 °C) were converted to the *in situ* temperature of −0.49 °C using an energy of activation of 48,821 J mol^{-1} determined from temperature gradient experiments (data not shown). Rates of macromolecular synthesis were converted to carbon production using 2.0×10^{18} cells mol^{-1} thymidine[42] and 1.42×10^{17} cells mol^{-1} leucine[43], in concert with a cellular carbon content of 11 fg C cell^{-1} (ref 44). For the sediment assays, a slurry was created by adding 1 g wet weight of sediment to 10 ml of 0.2 μm-filtered SLW water. The processing of the sediment slurries was identical to water samples except a total of three 80% v/v ethanol rinses were performed to enhance the removal of unincorporated substrate. After drying, 200 μl of tissue solubilizer (ScintiGest; Fisher Chemical) was added to each vial. The metabolic rate data were normalized per gram dry weight of sediment.

Dark CO_2 fixation was determined in sterile 40 ml glass vials filled to the top with sample (leaving no headspace) and capped with PTFE lined caps (10 and 5 live and 10 and 5 TCA-killed for casts 1 and 3, respectively). The vials were amended with sterile [^{14}C]bicarbonate (stock concentration = 0.1144 mCi ml^{-1}) to a final experimental concentration of 1 μCi ml^{-1} and incubated in the dark at 4 °C for 281 h (average). A separate time-course experiment (data not shown) revealed that incorporation was linear over this incubation period. Incubations were terminated by the addition of cold TCA (2.5% w/v final concentration) and filtering onto 0.2 μm polycarbonate filters. The filters were placed in 20 ml scintillation vials, acidified with 0.5 ml of 3N HCl, and dried at 60 °C for 24 h. Radioactivity on the filters was determined with a calibrated liquid scintillation counter following the addition of 10 ml of Cytoscint ES (MP Biomedicals).

Molecular and phylogenetic analysis of SSU rRNA gene sequences. DNA was extracted from a portion of each filter (1/8 of a 142 mm filter) using the Power Water DNA Isolation Kit and from sediments (~0.5 g wet weight) with the Power Soil DNA isolation kit (MO BIO Laboratories, Inc.). The extraction procedures followed those recommended by the manufacturer.

The SSU rRNA gene was amplified using the oligonucleotide primers 515F and 806R, as described previously[45]. Amplification reactions (50 μl each) were performed using 5 units of AmpliTaq Gold DNA polymerase LD (Invitrogen), 1× PCR Gold Buffer (Invitrogen), 3.5 mM $MgCl_2$, 10 pmol of each primer, 200 μM dNTPs, and 0.1–3 ng of DNA template. After 9 min of heat activation at 94 °C (AmpliTaq Gold DNA polymerase is a chemical hot-start enzyme), 35 cycles of PCR were performed using the following amplification conditions: denaturation at 94 °C for 45 s, annealing for 90 s at 50 °C, and elongation at 72 °C for 90 s, with a terminal elongation at 72 °C for 10 min. The optimum number of cycles for PCR was determined by successively lowering the cycle number so that false positive amplification was prevented while amplification was possible for the lowest biomass samples analysed. The concentration of the PCR products were determined using the Quant-iT Pico Green dsDNA Assay Kit (Invitrogen). The amplicons were pooled and cleaned with the MoBio UltraClean PCR Clean-Up Kit. Sequencing was performed using the Illumina MiSeq platform (Selah Genomics, Greenville, SC).

Paired end sequence reads were assembled and quality filtered using the Mothur[46] phylogenetic analysis pipeline (v1.33.2). The sequences were aligned with the SILVA Incremental Aligner[47] (SINA v1.2.11; database release 115). The aligned reads were checked for chimaeras using the Uchime algorithm[48], as implemented within Mothur, and chimaeric sequences were removed from the data. Sequences with >97% SSU rRNA gene sequence similarity were clustered into an OTU and representative sequences for each OTU were chosen for classification using the SILVA database. Diversity and richness estimates were calculated in Mothur[46]. Singletons were excluded from further analyses, and for simplicity of presentation, phyla represented by <1% of the sequence reads were grouped into the unclassified category (Fig. 2a). Community comparisons using Yue and Clayton theta similarity coefficient analysis and Weighted Unifrac were also performed within Mothur. MEGA 5.2 software was used for phylogenetic analysis using maximum likelihood, the Jukes–Cantor nucleotide substitution model (1,000 iterations), and a 253 nucleotide alignment. Attempts to detect SSU sequences from eukaryotes were based on previously published methods[50].

31. Carter, S. P. & Fricker, H. A. The supply of subglacial meltwater to the grounding line of the Siple Coast, West Antarctica. *Ann. Glaciol.* **53,** 267–290 (2012).
32. Horgan, H. J. *et al.* Subglacial Lake Whillans—Seismic observations of a shallow active reservoir beneath a West Antarctic ice stream. *Earth Planet. Sci. Lett.* **331–332,** 201–209 (2012).
33. Siegfried, M. R., Fricker, H. A., Roberts, M., Scambos, T. A. & Tulaczyk, S. A decade of West Antarctic subglacial lake interactions from combined ICESat and CryoSat-2 altimetry. *Geophys. Res. Lett.* 2013GL058616, doi:10.1002/2013GL058616 (2014).
34. Priscu, J. C. LTER Limno Methods Manual – MCM_Limno_Methods_current.pdf. http://www.mcmlter.org/data/lakes/MCM_Limno_Methods_current.pdf (2013).
35. Seeberg-Elverfeldt, J., Schlüter, M., Feseker, T. & Kölling, M. Rhizon sampling of porewaters near the sediment-water interface of aquatic systems. *Limnol. Oceanogr. Methods* **3,** 361–371 (2005).
36. American Public Health Association. *Standard methods for the examination of water and waste water* (American Public Health Society Press, 1995).
37. Costa, A. W. *et al.* Analysis of atmospheric inputs of nitrate to a temperate forest ecosystem from Δ^{17}O isotope ratio measurements. *Geophys. Res. Lett.* **38,** L15805 (2011).
38. Casciotti. K. L. Sigman, D. M., Galanter Hastings, M., Bohlke, J. K. & Hilkert, A. Measurement of the oxygen isotopic composition of nitrate in seawater and freshwater using the denitrifier method. *Anal. Chem.* **74,** 4905–4912 (2002).
39. Kaiser, J., Hastings, M. G., Houlton, B. Z., Rockmann, T. & Sigman, D. M. Triple oxygen isotope analysis of nitrate using the denitrifier method and thermal decomposition of N_2O. *Anal. Chem.* **79,** 599–607 (2007).
40. Fuhrman, J. & Azam, F. Thymidine incorporation as a measure of heterotrophic bacterioplankton production in marine surface waters: evaluation and field results. *Mar. Biol.* **66,** 109–120 (1982).
41. Kirchman, D., K'nees, E. & Hodson, R. Leucine incorporation and its potential as a measure of protein synthesis by bacteria in natural aquatic systems. *Appl. Environ. Microbiol.* **49,** 599–607 (1985).
42. Bell, R. T. Estimating production of heterotrophic bacterioplankton via incorporation of tritiated thymidine. In: Kemp, P. F., Sherr, B. F., Sherr, E. B. & Cole, J. J. (eds) *Handbook of Methods in Aquatic Ecology* (Lewis, 1993).
43. Chin-Leo, G. & Kirchman, D. Estimating bacterial production in marine waters from the simultaneous incorporation of thymidine and leucine. *Appl. Environ. Microbiol.* **54,** 1934–1939 (1988).
44. Kepner, R. L., Wharton, R., Jr & Suttle, C. A. Viruses in Antarctic Lakes. *Limnol. Oceanogr.* **43,** 1754–1761 (1998).
45. Caporaso, J. G. *et al.* Ultra-high-throughput microbial community analysis on the Illumina HiSeq and MiSeq platforms. *ISME J.* **6,** 1621–1624 (2012).
46. Schloss, P. D. *et al.* Introducing mothur: open-source, platform-independent, community-supported software for describing and comparing microbial communities. *Appl. Environ. Microbiol.* **75,** 7537–7541 (2009).
47. Pruesse, E., Peplies, J. & Glöckner, F. O. SINA: accurate high-throughput multiple sequence alignment of ribosomal RNA genes. *Bioinformatics* **28,** 1823–1829 (2012).
48. Edgar, R. C., Haas, B. J., Clemente, J. C., Quince, C. & Knight, R. UCHIME improves sensitivity and speed of chimera detection. *Bioinformatics* **27,** 2194–2200 (2011).
49. Holland, H. D. *The Chemistry of the Atmosphere and Oceans* (Wiley, 1978).
50. Amaral-Zettler, L. A., McCliment, E. A., Ducklow, H. W. & Huse, S. M. A method for studying protistan diversity using massively parallel sequencing of V9 hypervariable regions of small-subunit ribosomal RNA genes. *PLoS ONE* **4,** e6372 (2009).

Extended Data Table 1 | Crustal and seawater components to SLW waters

	μeq L^{-1}							
Sample	Na^+	K^+	Mg^{2+}	Ca^{2+}	F^-	Cl^-	SO_4^{2-}	HCO_3^-
SLW Average *	5276	186	507	859	31.5	3537	1111	2111
Sea water component †	3038	66	691	132	0.4	3537	366	16
Non-seawater, crustal weathering component ‡	2239	120	-183 §	726	31.1	0	745	2096

* Average values for hydrocasts 1, 2 and 3.
† Calculated using Cl^- concentrations and ratios of each species to Cl^- in seawater in μeq l^{-1}; Na^+ 0.859, K^+ 0.019, Mg^{2+} 0.195, Ca^{2+} 0.037, F^- 0.00013, SO_4^{2-} 0.103, and HCO_3^- 0.004 (ref. 49).
‡ Calculated by subtracting the seawater component from the average SLW solute concentration for each ion.
§ Negative values indicate the potential for ion exchange of Mg^{2+} with other cations on clay minerals present in suspended sediments of SLW.

Extended Data Table 2 | Summary of parameters for the SLW SSU gene sequence data

Site	Number of Sequences *	Number of OTUs †	Coverage ‡	Inverse Simpson Diversity Index ‡	Shannon Diversity Index ‡	Chao Richness Estimator ‡
Drill and borehole water	984,412	962	99.8%	11.0	3.4	5,370
SLW water column	2,686,526	3,931	99.5%	35.3	4.9	41,603
SLW sediments	333,600	2,424	97.3%	31.8	5.1	42,079

* Sequences remaining after quality filtering, and removal of chimaeric sequences and singletons.
† OTUs that passed quality filtering, excluding singletons.
‡ Calculated using Mothur[46].